Pioneer. Adv. Mater. 2026, 2(1): 1-18 DOI: 10.48308/piadm.2026.245775.1030

Shahid Beheshti University

Pioneering Advances in Materials

Journal homepage: http://piadm.sbu.ac.ir ISSN: 3115-7114

Research paper

Modulating Dye–Surfactant Interplay: How Trypan Blue Concentration and Droplet Loading Redefine the Photophysics and Nanostructure of Surfactant-Stabilized Water-in-Oil Microemulsions

Masoumeh Samani[1], Mehrdad Moradi[1]*, Abbas Rahdar[2]

[1]*Institute of Nanoscience and Nanotechnology, University of Kashan, Kashan, 87317, Iran*
[2]*Department of Physics, University of Zabol, Zabol, 538-98615, Iran*

*m.moradi@kashanu.ac.ir

Article info:

Article history:

Received: 05/08/2026

Accepted: 24/08/2026

Keywords:

W/O microemulsions, Nanodroplets, Trypan Blue, Hypsochromic shift, Photophysical properties

Abstract

In this study, aqueous nanodroplets with different concentrations of the dye Trypan Blue are synthesized and investigated within W/O microemulsions. The AOT surfactant is used to stabilize the resulting nanodroplets in n-hexane solvent. The molar ratio of water to surfactant is kept constant to evaluate the role of Trypan Blue concentration on the photophysical and structural properties of the microemulsions using various characterization techniques. Additionally, these systems are studied at different mass fractions of droplets (MFD). DLS data indicate that the hydrodynamic diameters of the nanodroplets range between 109 and 169 nm, while also showing that the droplet size decreases with increasing Trypan Blue content. Furthermore, PDI values range from 0.138 to 0.201, indicating moderate polydispersity of the synthesized particles. The UV-Vis spectra show a hypsochromic shift in λ_{max} from 562 to 594 nm, corresponding to a decrease in polarity within the confined droplet medium. Moreover, the absorption intensity is found to increase for higher MFD values. The fluorescence spectroscopic results reveal that increasing MFD is accompanied by an enhancement in emission intensity, whereas no significant change occurs in the emission wavelength. The calculations show that $E_T(30)$ values range from 48.1 to 50.9 kcal/mol, indicating a lower polarity of the droplet core compared to bulk water. Overall, the findings suggest that the photophysical properties of these microemulsions can be optimized and controlled, with desirable stability observed at moderate dye concentrations and MFD levels.

1. Introduction

Emulsions are considered a class of heterogeneous colloidal systems. In these systems, immiscible liquid phases are combined, and the dispersed phase is distributed within the continuous phase as droplets with micrometer-scale dimensions [1–3]. Although these systems appear kinetically stable, the absence of stabilizing agents such as emulsifiers leads to phase separation over time. Phase separation may occur through mechanisms such as droplet coalescence, creaming, or Ostwald ripening, all of which are influenced by Gibbs free energy and van der Waals interactions [4, 5]. In comparison with conventional emulsions, microemulsions are considered a special class of these systems and are thermodynamically stable. They typically exhibit characteristics such as isotropy, optical transparency due to minimal Rayleigh light scattering, and relatively low viscosity [6, 7]. In contrast to macroemulsions, which require high mechanical energy for formation and possess limited stability, microemulsions form spontaneously and remain stable over time. This characteristic arises from the flexible interfacial film model. According to this model, the energy required to bend the surfactant layer (characterized by the bending modulus $\kappa \approx kT$) is considered a key factor [8, 9]. In general, microemulsions are classified into three main types: oil-in-water (O/W), water-in-oil (W/O), and bicontinuous systems [10, 11]. In W/O microemulsions, also known as reverse micelles, nanodroplets of the aqueous phase are enclosed within a continuous oil phase. Such systems have wide-ranging applications; for example, they are used as templates in the synthesis of metallic nanoparticles, in drug delivery systems, and in the simulation of biological processes such as the modeling of cellular membranes [12–15]. Surfactants, which possess an amphiphilic nature, play a key role in the formation and stability of microemulsion systems. These substances play an important role in enhancing system stability by reducing the interfacial tension according to the Gibbs adsorption equation and by regulating the curvature of the interfacial film [16–18]. Depending on the charge of the hydrophilic group, surfactants are classified into four main categories: anionic, cationic, nonionic, and amphoteric [19, 20].Sodium 1,4-bis(2-ethylhexyl) sulfosuccinate (AOT) is an anionic surfactant containing two hydrocarbon chains that is widely used in W/O systems. This compound can form reverse micelles and reduce interfacial tension significantly, eliminating the need for a cosurfactant. In such systems, the hydrophilic sulfonate head group is oriented towards the aqueous core, while the hydrophobic alkyl chains extend into the oil phase. As a result of this arrangement, a core–shell structure is formed. In this structure, the balance between electrostatic and hydrophobic interactions leads to thermodynamic stability [21–23]. In AOT-based W/O microemulsions, water nanodroplets are formed that are covered by a surfactant monolayer. This surfactant layer stabilizes the nanodroplets through both electrostatic charges and steric barriers, thereby preventing their coalescence. As a result, the solubilization capacity of hydrophilic compounds in nonpolar media increases, and properties such as viscosity and polarity are modified [24–26]. Adding dyes to W/O microemulsions converts them into sensitive probes for studying molecular interactions and photophysical phenomena [27, 28]. Encapsulating inorganic pigments such as Prussian blue and cadmium sulfide within these systems increases their stability against light and oxidation. For this reason, these materials are used in applications such as inks, coatings, and sensors [29-31]. In previous studies, researchers have investigated various dyes, including methylene blue and carotenoids.

These dyes improve the dyeing quality of wool by increasing solubility in hydrophobic media and allow for a more precise understanding of oxidation reactions [32–38]. Trypan blue is a hydrophilic, acidic azo dye widely utilized as a vital stain to accurately assess cell viability. Due to its inability to penetrate intact cell membranes, only damaged or necrotic cells are stained by this dye.

This property has enabled the application of trypan blue in cytotoxicity assays, histological studies, and ophthalmic surgeries. In addition, Trypan blue exhibits a maximum absorption around 600 nm, and its high sensitivity to changes in the media is one of its important characteristics. These features make Trypan blue an ideal probe for investigating confined systems such as microemulsions [39–42].

In this study, aqueous nanoemulsions containing different concentrations of trypan blue dye are prepared and investigated in AOT-based W/O systems. In this regard, the relevant conditions and parameters are optimized to obtain stable nanodroplets with sizes below 50 nm. Furthermore, the dye's encapsulation capacity and stability, along with the system's characteristics, are carefully examined to precisely determine their impact on various factors.

2. Experimental section

2.1. Chemicals and apparatus

All chemicals and solvents were purchased from Sigma-Aldrich and used in analytical-grade purity. The particle size distribution in water-in-oil (W/O) microemulsions was measured using the Dynamic Light Scattering (DLS) technique with a VASCO 2 instrument manufactured by Cordouan Technologies.

The ultraviolet–visible (UV–Vis) absorption spectra were obtained using a Cary 100 spectrophotometer (Agilent Technologies). This double-beam instrument measures absorbance with high precision over the wavelength range of 190 to 900 nm. Photoluminescence (PL) emission spectra were measured using a Cary Eclipse Spectrophotometer (Agilent Technologies).

2.2. Preparation of water nanodroplets containing Trypan Blue using AOT

To prepare aqueous nanodroplets using the AOT surfactant with various concentrations of Trypan Blue dye, the following procedure was followed. First, a precise amount of Trypan Blue powder was dissolved in deionized water to obtain aqueous solutions with the desired concentrations.

The dye content in the microemulsion was determined based on the mass ratio of Trypan Blue to water. Subsequently, accurately measured amounts of AOT surfactant, n-hexane oil, and the dye-containing aqueous solution were mixed to form AOT reverse microemulsions, while maintaining a constant water-to-surfactant molar ratio (W = 20).

All steps were performed under strictly controlled conditions to ensure the formation of uniform and stable nanodroplets.

In the final step, the microemulsion was diluted with n-hexane oil so as to achieve a specific mass fraction of nanodroplets.

This process led to the formation of nanoparticles exhibiting the desired properties at ambient temperature.

3. Results and discussion

In this section, the analyses and experimental data related to the synthesized microemulsions are presented and discussed.

These systems were prepared with a constant molar ratio of water to surfactant (W = 20) and different dye-to-water mass ratios (m_{dye}/m_{water} = 0.0000625, 0.00025, 0.001, and 0.01).

In addition, the mass fraction of droplets (MFD) was considered at 0.01, 0.03, and 0.07.

3.1. Particle size distribution by dynamic light scattering (DLS)

The DLS analysis results of the synthesized systems indicate that their hydrodynamic diameters lie within the range of 109 to 169 nm.
Moreover, the findings indicate that as the dye concentration in the solution increases, the droplet size gradually decreases.
This is likely due to the enhanced electrostatic repulsive force caused by the sulfonate groups present in the dye molecules. Furthermore, as the mass fraction of droplets (MFD) increases from 0.01 to 0.03, a gradual decrease in the average droplet size is observed. This phenomenon may be associated with an increased droplet number density in the system, resulting in more efficient packing, or with a slight reduction in droplet coalescence in relatively dilute media. The polydispersity index (PDI) values range from 0.138 to 0.201.
This range indicates a droplet size distribution with moderate polydispersity. This type of dispersion is a common characteristic of microemulsion systems. Additionally, PDI values below 0.2 indicate a relatively uniform and acceptable droplet size distribution. The presence of bimodal or trimodal distributions in some of the graphs indicates the coexistence of different particle populations within the system, which may arise from the presence of smaller free micelles or larger droplet aggregates. This behavior is likely due to interactions between dye molecules and surfactant molecules.

Table 1. Z-average and PDI values obtained from the DLS analysis

3	MFD = 0.01		MFD = 0.03	
	Z-avg (nm)	PDI	Z-avg (nm)	PDI
0.0000625	168.65	0.19555	134.85	0.18472
0.00025	152.47	0.14575	142.41	0.13831
0.001	119.3	0.17124	109.23	0.20072

Additionally, Table 1 presents the Z-average values and PDI indices obtained from the cumulants analysis.
Figures 1 to 3 present the particle size distribution obtained using three analytical methods (SBL, cumulants, and Padé–Laplace) under three modes: intensity-weighted, number-weighted, and volume-weighted.
Figure 1, which shows the results of the SBL analysis, the intensity-weighted plots (Figure 1a, d, g) generally exhibit bimodal distributions, indicating the presence of particles with different sizes within the system.
By comparing between the results of different MFD values, one can find that the variations in this parameter is capable of affecting the overall particle size distribution.
Meanwhile, at lower MFD values, a more balanced distribution of particle size is achieved when the contributions of the two particle populations are more comparable. Moreover, the particle size distribution is found to significantly depend on the dye concentration.
In other words, at lower dye concentrations, the particle sizes become non-uniform, so that several distinct populations of particles (having different sizes) are observed, suggesting that the interactions occurring between the system components can be changed under more dilute conditions.
Accordingly, the formation of structures with various size distributions is expected to be increased. In the number-weighted plots for the SBL mode (Figure 1b, e, h), smaller particles exhibit a dominant contribution, and the distributions are generally simpler and closer to unimodal. These results indicate the presence of a large number of small particles in the system. In contrast, in the volume-weighted plots (Figure 1c, f, i), the contribution of larger particles becomes slightly more significant. Nevertheless, smaller particles still constitute the majority of the overall size distribution.

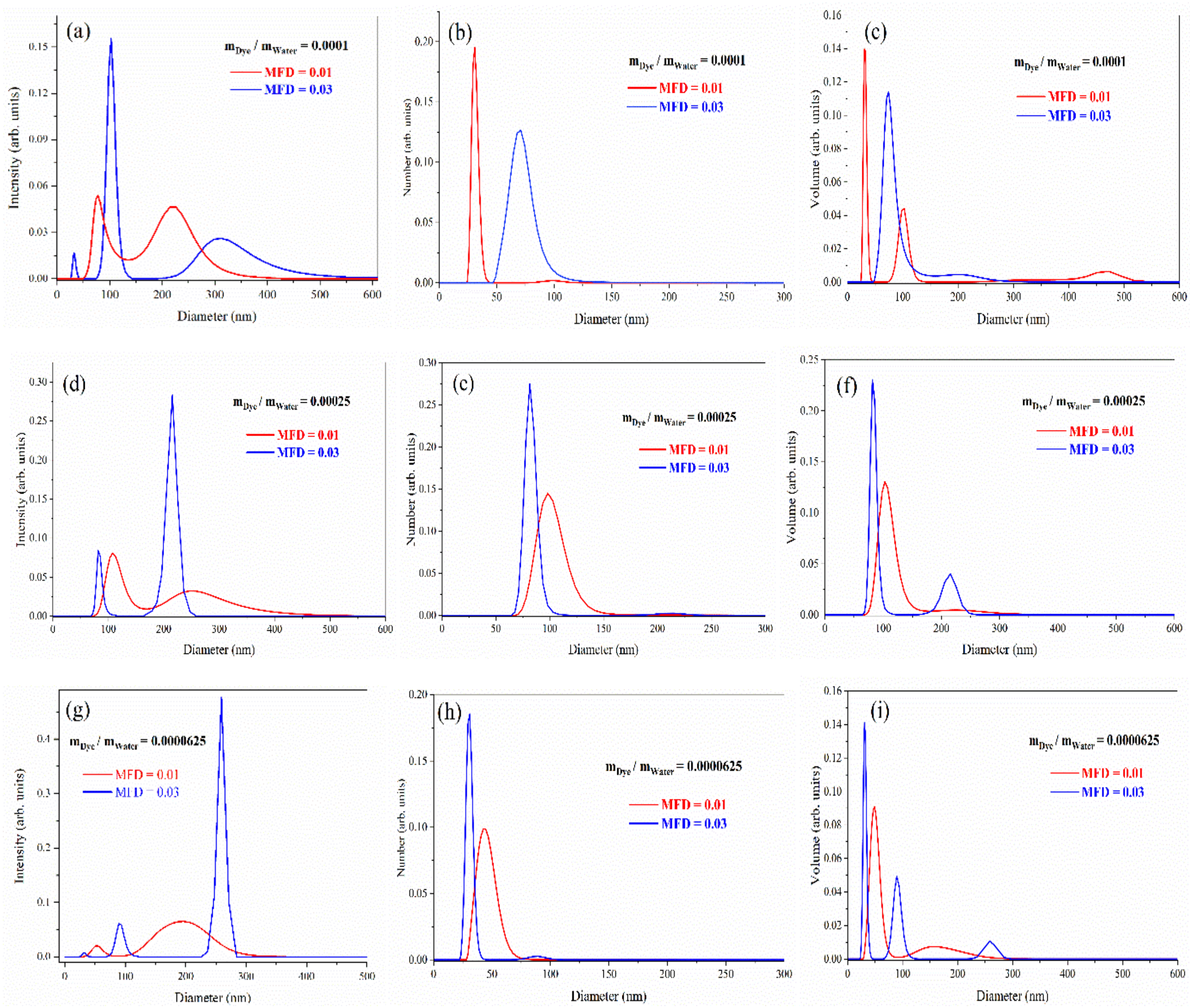

Figure 1. Particle size distribution based on SBL analysis for different concentrations of trypan blue (m_{dye}/m_{water} = 0.001 (a–c), 0.00025 (d–f), and 0.0000625 (g–i))

In Figure 2, which presents the results of the cumulants analysis, the intensity-weighted distributions (Figure 2b, e, i) predominantly exhibit broad unimodal profiles and, in some cases, weak bimodal behavior. Increasing dye concentration and droplet mass fraction lead to a shift of the distribution peaks toward smaller particle sizes. Furthermore, PDI values exceeding 0.18 indicate particle size heterogeneity, which is likely attributed to droplet swelling induced by the dye. In addition, in the number-weighted (Figure 2a, d, g) and volume-weighted (Figure 2c, f, h) representations, the distributions become narrower as the MFD increases. Based on these findings, the cumulants method is less sensitive to the true multimodal nature of the distribution of the particle sizes, although it can effectively capture the overall trend observed in size variations. In Figure 3, corresponding to the Padé–Laplace analysis, the intensity-weighted distributions (Figure 3a, d, g) are predominantly bimodal, with one peak located at larger sizes (approximately 200–250 nm) and a second peak at smaller sizes (approximately 60–110 nm). In the number-weighted distributions (Figure 3b, e, h), a single dominant peak is generally observed in the range of 65–108 nm. Similarly, in the volume-weighted distributions (Figure 3c, f, i), the contribution of smaller particles is greater than that of larger ones.

Overall, the DLS analysis revealed that the formed nanodroplets possess sizes below 200 nm and exhibit good stability. On the basis of these findings, one can infer that the increase in the dye concentration can alter the interfacial region, giving rise to a considerable decrease in the particle size.

Additionally, the particle size distribution profile as well as the number of peaks observed in the distributions can be significantly influenced by the MFD value.

3.2. UV-Vis absorption spectroscopy

The electronic transitions and solvatochromic behavior of Trypan Blue within aqueous nanodroplets in the synthesized microemulsion systems were investigated in the present study using UV–Vis spectroscopy, thus allowing for the evaluation of the confinement of Trypan Blue inside water nanodroplets that can influence its absorption characteristics.

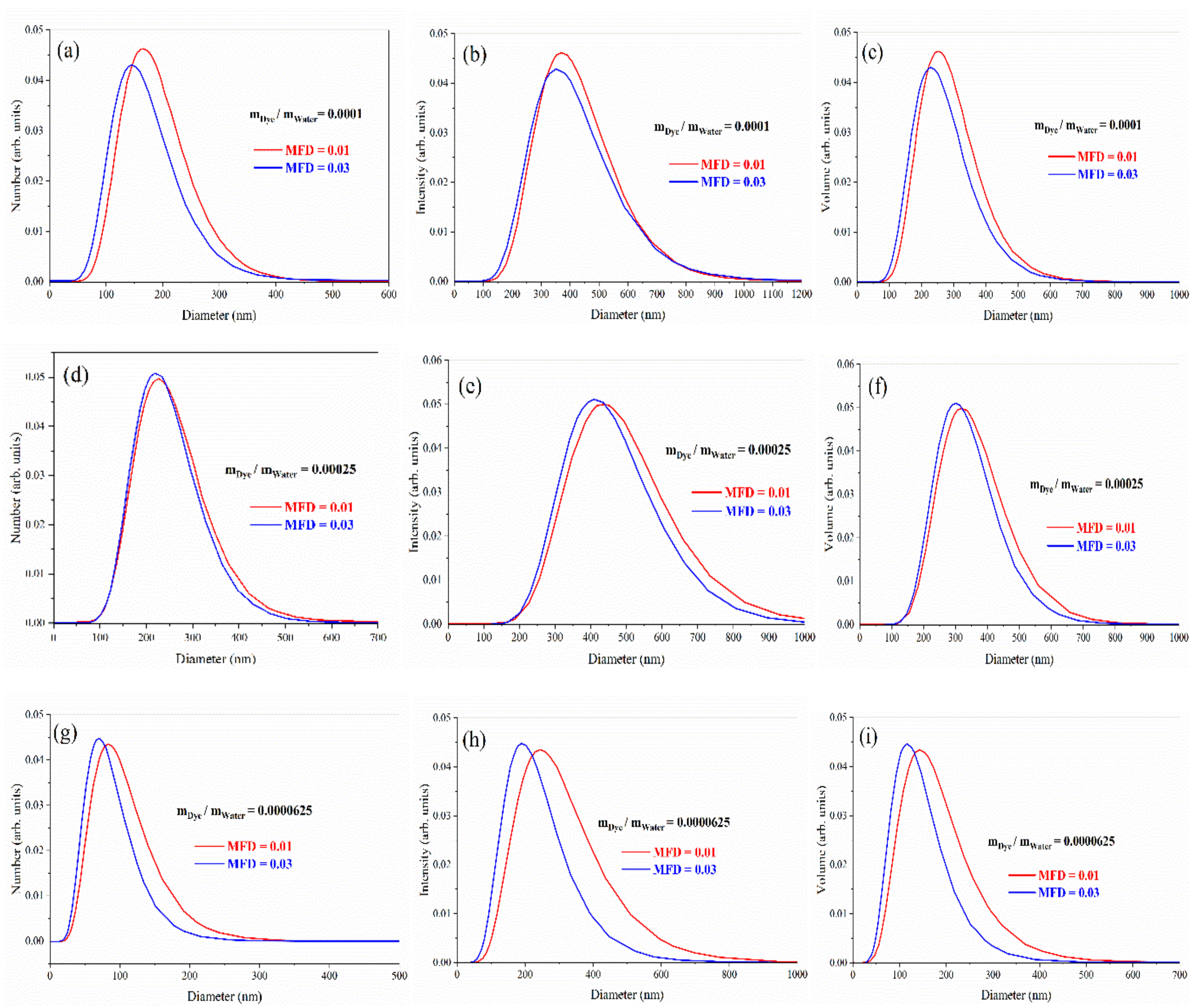

Figure 2. Particle size distribution based on cumulants analysis for different concentrations of trypan blue (m_{dye}/m_{water} = 0.001 (a–c), 0.00025 (d–f), and 0.0000625 (g–i))

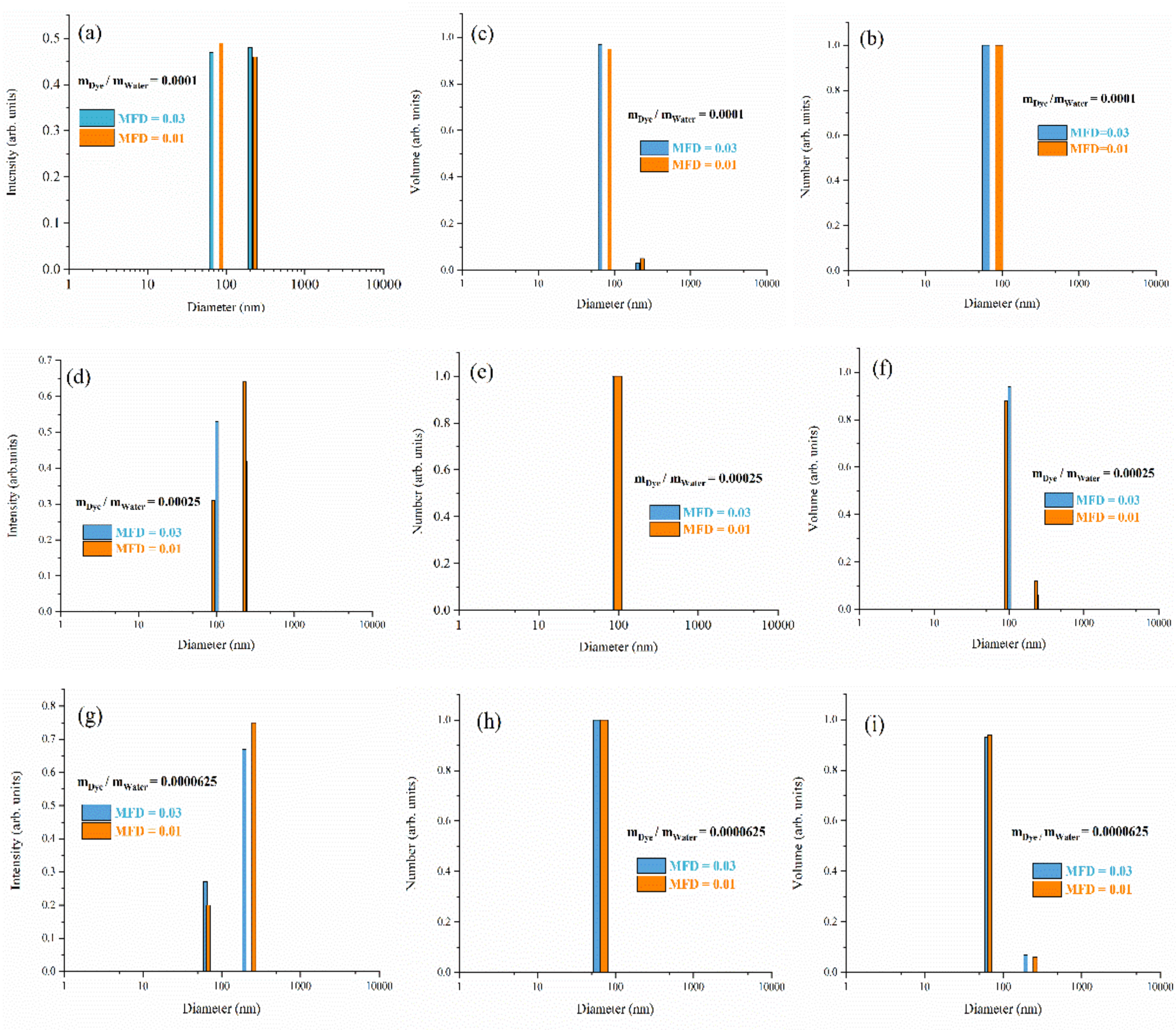

Figure 3. Particle size distribution based on Padé–Laplace analysis for different concentrations of trypan blue (m_{dye}/m_{water} = 0.001 (a–c), 0.00025 (d–f), and 0.0000625 (g–i))

In fact, Trypan Blue is an azo dye with well-defined electronic transitions of the following types: n→π* and π→π*. These transitions are typically capable of producing a broad absorption band in the visible region, which can be efficiently utilized as a suitable probe for examining polarity and microenvironmental conditions in various systems. By monitoring changes occurring in absorbance intensity and λ_{max}, valuable information about the extent of dye solubilization is obtained. Moreover, the possibility of intermolecular interactions and aggregation among dye molecules, along with the solvent medium effect on the spectral characteristics can be investigated, thereby complementing the results extracted from the DLS analysis. In this way, it is possible to make a correlation between the droplet size and optical behavior of the system, providing a more comprehensive understanding of the characteristics of the microemulsions. The average λ_{max} and absorbance intensity values obtained for different dye concentrations and

MFD values are presented in Table 2. The results indicate that the λmax values of the synthesized systems are in the range of 562–594 nm. Compared with free Trypan Blue in water ($\lambda_{max} \approx$ 607 nm), these systems exhibit a shift toward shorter wavelengths, commonly referred to as a hypsochromic (blue) shift.

This observation suggests that Trypan Blue is located within the nanodroplet core in an medium of lower polarity.

Furthermore, the ability of the dye to form hydrogen bonds significantly decreases, arising from its incorporation into the microemulsion structure and its interactions with surfactant molecules. Moreover, by increasing the dye concentration and MFD value, the absorbance intensity increases, thus generally following the Beer–Lambert law. Nevertheless, the absorbance behavior is found to deviate from linearity at higher concentrations, which can be attributed to phenomena such as dye aggregation or self-quenching.

Table 2. Mean values of the maximum absorption wavelength (λ_{max}) and absorbance intensity obtained from UV–Vis spectra

MFD	m_{dye}/m_{water}	λ_{max} (nm)	Absorbance Intensity
0.01	0.0000625	587	0.7
	0.00025	587	0.38
	0.001	588	0.13
	0.01	585	0.35
0.03	0.0000625	589	0.027
	0.00025	585	0.18
	0.001	584	0.33
	0.01	580.6	0.93
0.07	0.0000625	594	0.076
	0.00025	562	0.36
	0.001	584.6	0.83
	0.01	581.6	1.79

The UV–Vis absorption spectra and the corresponding intensity distribution curves for different dye concentrations at three MFD values are presented in Figure 4.

As observed, all spectra exhibit a broad peak within the range of 550–650 nm, which is attributed to the π–π* transition of the azo group. In addition, weak shoulders are also detected, which are likely associated with vibronic coupling or the formation of dye dimers.

At the highest concentration investigated, increasing the MFD value is accompanied by noticeable changes in the absorption spectra; the spectra gradually broaden and the absorbance intensity increases. This behavior is likely due to the increased number density of nanodroplets. By increasing the nanodroplet density, the effective concentration of dye molecules within the microemulsion medium becomes higher, thereby affecting the behavior of the overall system. Furthermore, by increasing MFD, a slight shift occurs toward shorter wavelengths (i.e., hypsochromic or blue shift), thereby decreasing λ_{max} from 585 to approximately 582 nm at a mass fraction of 0.01 (Figure 4a,b). This shift can be attributed to enhanced electrostatic interactions between the dye molecules and the surfactant molecules within the system. As a result of these interactions, the polarity of the droplet's internal medium is slightly decreased. This reduction in polarity leads to enhanced stabilization of the dye molecule's ground state relative to its excited state. At concentration of 0.001 (Figure 4c,d), λ_{max} remains essentially constant, while the absorbance intensity increases with increasing of MFD, indicating that the dye molecules show a low propensity for aggregation under these conditions, and that the encapsulation process proceeds efficiently. Moreover, based on the intensity distribution plot depicted in Figure 4d, narrower peaks are observed at lower MFD values, suggesting a more homogeneous microenvironment.

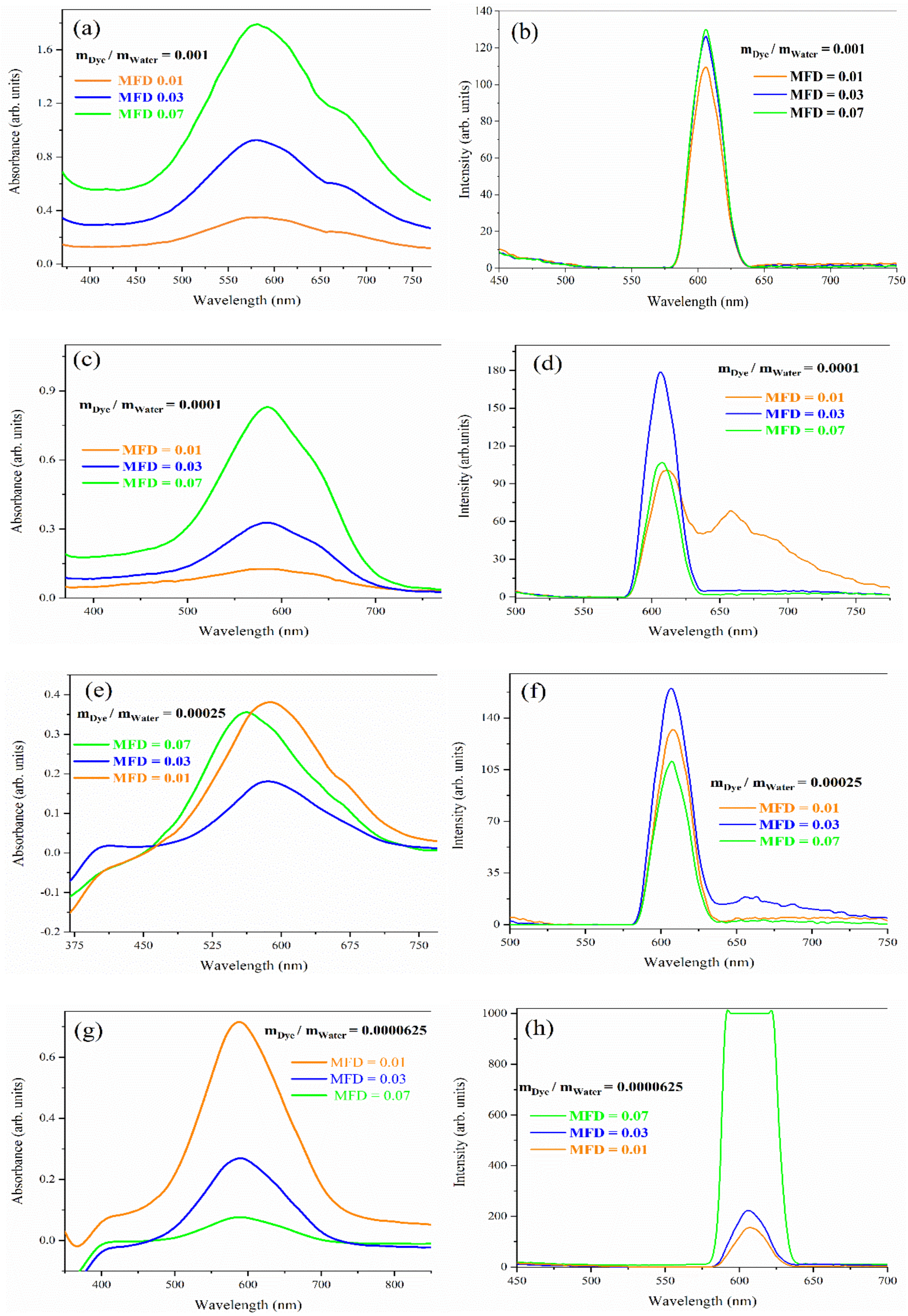

Figure 4. UV–Vis absorption spectra and corresponding intensity distributions for different concentrations of Trypan Blue with m_{dye}/m_{water} mass ratios of 0.01 (a, b), 0.001 (c, d), 0.00025 (e, f), and 0.0000625 (g, h) at various MFD

When the concentration is 0.00025 (Figure 4e,f), an unexpected shift occurs toward shorter wavelengths, giving rise to λ_{max} of 562 nm at a mass fraction of 0.07. This phenomenon may result from specific solvent–medium effects or from changes in the dispersion state of the dye at very low concentrations.

In this case, the absorbance intensity falls within a moderate range of approximately 0.18–0.36 a.u. At the lowest concentration, 0.0000625 (Figure 4g, h), λ_{max} shifts toward longer wavelengths, reaching approximately 594 nm at a mass fraction of 0.07.

This shift may be associated with an increase in the effective polarity of the medium within more dispersed droplets. In addition, due to the extremely low dye loading, the absorbance intensity remains relatively low, within the range of about 0.027–0.7 a.u. Overall, these observations are fully consistent with the principles of solvatochromism in microemulsion systems.

In such systems, the electronic medium of the dye is altered by the interfacial region created by the surfactant molecules, leading to spectral shifts in the absorption band similar to those observed for dyes dissolved in mixed solvent media. On the other hand, DLS data indicate that the droplet size decreases with increasing dye concentration, which is accompanied with the hypsochromic shifts in the absorption spectra. In other words, the mobility of water molecules is restricted by smaller droplets within the aqueous core, giving rise to a change in the effective polarity of the microenvironment and the absorption behavior of the dye.

Accordingly, the photophysical properties of the system can be efficiently controlled and tuned by changing the formulation parameters, taking into account the agreement observed between the DLS and UV–Vis results.

3.3. Fluorescence spectroscopy

The fluorescence spectroscopy was used to investigate photophysical behavior of Trypan Blue in the synthesized microemulsion systems, allowing for a more detailed examination of processes such as molecular behavior in the excited state, solvent relaxation, and energy transfer mechanisms. Under the assumed conditions, the emission spectra are indicative of detectably weak fluorescence for the dye Trypan Blue.

It should be noted that, Trypan Blue is basically non-fluorescent or shows incredibly weak emission in pure aqueous media, which can be assigned to the presence of efficient non-radiative relaxation pathways in water. In this case, the energy absorbed is dissipated as heat instead of emitting as light. By encapsulating the dye in the aqueous microemulsion's nanodroplets, the molecular motions and relaxation pathways are restricted, thereby leading to an increase in the fluorescence intensity. Essentially, while the maximum emission wavelength is found to remain unchanged under these conditions, the fluorescence intensity varies as a function of the dye concentration and droplet mass fraction. In this regard, the emission wavelength (λ_{em}) and photoluminescence intensity obtained for different Trypan Blue concentrations at various MFD values are presented in Table 3, demonstrating the roles of MFD and dye concentration in the approximate quantum yield and polarity-dependent variations of the microenvironment. The absorption and emission spectra of Trypan Blue with various concentrations at three different MFD values, along with the calculated Stokes shifts are shown in Figure 5. As can be seen, the emission bands in the 600 nm to 650 nm ranges are broad and somewhat asymmetric, being in agreement with charge transfer states typically taking place in azo dyes. At low concentrations (e.g., 0.0000625), the fluorescence intensity increases with increasing MFD values, according to Figure 5(j–l).

Table 3. The results obtained from fluorescence spectra of Trypan Blue with different concentrations at various MFD values

MFD	Concentration (m_{dye}/m_{water})	λ_{em} (nm)	PL Intensity (a.u.)
0.01	0.0000625	607	155
	0.00025	608	132
	0.001	611.5	100.79
	0.01	606	109
0.03	0.0000625	606	223
	0.00025	606.5	160
	0.001	606	178
	0.01	606	126
0.07	0.0000625	607	1000
	0.00025	607	110.56
	0.001	607.5	106.7
	0.01	606	130

This variation behavior is indicative of an increase in the number of droplets, and a decrease in the fluorescence quenching between them, resulting in stronger emission. Meanwhile, the Stokes shift observed approximately between 20 and 21 nm implicates limited freedom of movement and rearrangement of the solvent molecules surrounding the excited state, arising from the presence of a hydrophobic and constrained microenvironment.

At a concentration of 0.0001, the spectra in Figure 5 (d–f) show a similar trend compared to that seen at lower concentrations, essentially indicating unchanged photophysical properties of the system within this concentration range. In the case of intermediate concentrations (e.g., 0.00025 (Figure 5g–i) and 0.001 (Figure 5a–c)), one can see an inverse relationship between the dye concentration and fluorescence intensity. By increasing the dye concentration and keeping the MFD constant, a decrease occurs in the fluorescence intensity, suggesting that the dye molecules within the aqueous core approach each other more closely at higher concentrations. This, in turn, promotes self-absorption or excimer formation processes, which can ultimately lead to the fluorescence quenching. In addition, by increasing the MFD values, the fluorescence intensity slightly increases, likely due to a higher number of droplets in the system and enhanced amount of emitted light.

Alternatively, the emission maximum (λ_{em}) shows a slight shift toward longer wavelengths (i.e., a red shift) when increasing the dye concentration, which can be attributed to changes in the local environment around the dye molecules with stabilized excited states at higher concentrations. These findings well accord with the UV–Vis analysis and confirm the reliability of the results.

For higher dye concentrations and MFD values, the absorption band is observed to shift towards shorter wavelengths, indicating a reduction in environmental polarity and aligning well with the relatively small Stokes shifts found here. This behavior reflects limited energy loss in lower-polarity cores. On the other hand, the increase in fluorescence intensity at higher MFD values is in good agreement with DLS data as well. In this respect, non-radiative decay pathways are reduced by smaller or more uniform droplets, which can in turn enhance the fluorescence quantum yield.

3.4. Solvatochromic effects, polarity parameter ($E_T(30)$), and photophysical dynamics

The solvatochromic effects of Trypan Blue on the synthesized systems were precisely investigated by utilizing a set of commonly used physicochemical relationships, each of which gives valuable information with respect to the solvent reorganization, polarity of the medium, and variations in the dipole moment between electronic states. Table 4 presents the aforementioned relationships.

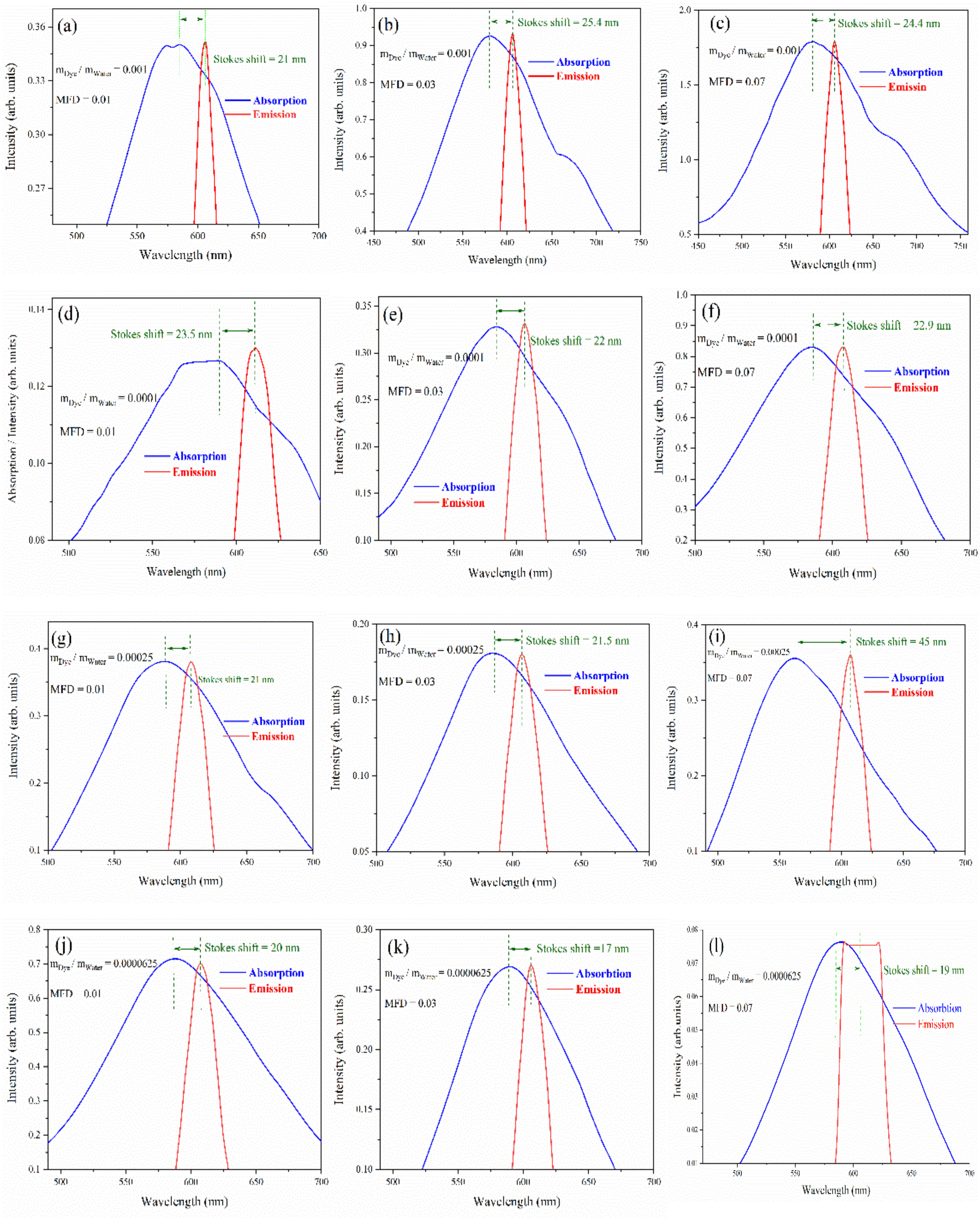

Figure 5. Absorption and emission spectra obtained from Trypan Blue with different concentrations (m_{dye}/m_{water}) of: 0.001 (a-c), 0.0001 (d-f), 0.00025 (g-i), and 0.0000625 (j-l) at various MFD values

Table 4. The equations and formulas used for determining photophysical properties and solvatochromic effects of Trypan Blue on W/O microemulsions

Entry	Equation	Formula
Eq. 1	Polarity Parameter ($E_T(30)$)	$E_T(30) = \frac{28591}{\lambda_{max}}$
Eq. 2	Stokes shift (Δλ or Δν)	$\Delta v = 10^7 \times (\frac{1}{\lambda_{max}} - \frac{1}{\lambda_{em}})$
Eq. 3	Lippert–Mataga equation	$\Delta v = \frac{2(\mu_e - \mu_g)^2}{hca^3} f + constant$
Eq. 4	Orientation polarizability function	$f = \frac{\varepsilon - 1}{2\varepsilon - 1} - \frac{n^2 - 1}{2n^2 - 1}$

Based on the equations provided in Table 4, Reichardt polarity parameter $E_T(30)$, Stokes shift (Δλ and Δν), and the dipole moment ratio (μg/μe) were calculated for different concentrations of Trypan Blue at various MFD values, and the results obtained are summarized in Table 5.

As can be inferred, the $E_T(30)$ parameter is ranged from 48.1 to 50.9 kcal/mol, indicating that the polarity of the medium in these systems is lower than that of bulk water due to the confinement of water nanodroplets by the AOT surfactant. In fact, the aqueous nanodroplets are encapsulated by the surfactant molecules, thus allowing for the phase separation between the aqueous and organic domains. At low concentrations of Trypan Blue (e.g., 0.0000625) and high mass fractions, the calculated $E_T(30)$ value is found to be reduced to about 48.1 kcal/mol, indicating a decrease in the polarity of the medium. This behavior is likely due to the increased droplet density and enhanced inter-droplet interactions, which may ultimately lead to an enhancement in the hydrophobic character of the microemulsion system. Despite the aforementioned decrease in $E_T(30)$ value, it remarkably increases to approximately 50.9 kcal/mol at a concentration of 0.00025 and the same mass fraction, most likely due to the preferential aggregation of dye molecules within specific regions of the system. This, in turn, changes the local polarity of the medium. With regard to the calculated Stokes shifts, one can observe moderate values, being consistent with the typical behavior of azo dyes in structured media. For intermediate concentrations (e.g., 0.00025) and higher mass fractions, the Stokes shift increases, likely arising from the aggregation of dye molecules and the subsequent enhanced solvent relaxation processes. This observation agrees with the above-mentioned reduction in fluorescence intensity. Furthermore, the calculated dipole moment ratios are found to be close to unity, suggesting the presence of a relative balance in polarity between the ground and excited states. Additionally, the dipole moment ratios slightly increase with increasing MFD, revealing a limited intramolecular charge transfer within the synthesized microemulsion systems.

The variations of $E_T(30)$ and Stokes shift as a function of MFD are presented in Figure 6. As can be seen, the microemulsion system shows nonlinear behavior at higher concentrations. In the case of high MFD values and low dye concentrations, $E_T(30)$ decreases noticeably. However, at the same MFD and intermediate concentrations, the Stokes shift is observed to increase significantly. These results are indicative of the possible dye molecule aggregation within the system, being consistent with the DLS and

UV–Vis measurements. In other words, according to the DLS results, the droplet size decreases with increasing the concentration, which can be related to the increases in $E_T(30)$ and $\Delta\nu$ values. Importantly, the reduced mobility of water molecules and stronger hydrogen-bonding interactions between the dye and the surfactant cause the polarity of the core to be increased. Similarly, based on the UV–Vis spectra, the hypsochromic shifts accompanied with λ_{max} reduction when increasing MFD are consistent with lower $E_T(30)$ values.

Moreover, fluorescence intensity is enhanced for higher MFD values, indicating that the contribution of non-radiative decay pathways is reduced in less polar media.

Overall, under intermediate mass fractions and concentrations, an appropriate equilibrium can be achieved between stability and photophysical behavior, thereby effectively tuning the microemulsion polarity.

In this way, the resulting microemulsion systems may represent themselves as promising candidates for therapeutic or imaging applications.

Table 5. Solvatochromic parameters calculated for Trypan Blue in W/O microemulsions

MFD	Dye Concentration (m_{dye}/m_{water})	$E_T(30)$ (kcal/mol)	$\Delta\lambda$ (nm)	$\Delta\nu$ (cm^{-1})	μ_g/μ_e
0.01	0.0000625	48.71	20.0	561.3	0.9
	0.00025	48.71	21.0	588.4	0.9
	0.001	48.62	23.5	653.6	1.0
	0.01	48.87	21.0	592.4	0.9
0.03	0.0000625	48.54	17.0	476.3	0.8
	0.00025	48.87	21.5	606.0	0.9
	0.001	48.95	22.0	621.6	1.0
	0.01	49.24	25.4	721.9	1.1
0.07	0.0000625	48.13	19.0	360.6	0.8
	0.00025	50.87	45.0	1319.1	1.2
	0.001	48.90	22.9	644.8	1.0
	0.01	49.16	24.4	692.3	1.1

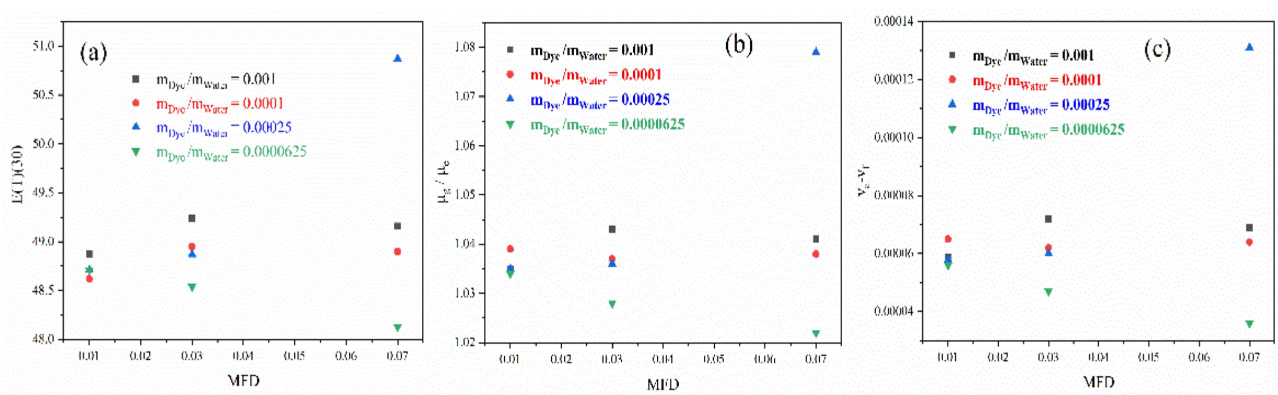

Figure 6. Photophysical properties of Trypan Blue with respect to MFD for W/O microemulsions: (a) $E_T(30)$, (b) dipole moment ratio (μ_g/μ_e) and (c) Stokes shift ($\Delta\nu$)

4. Conclusion

In conclusion, W/O microemulsions containing the dye Trypan Blue have been stabilized by AOT and thoroughly characterized. The formation of aqueous nanodroplets with sizes below 200 nm and acceptable stability was confirmed by DLS analysis.

Furthermore, the hydrodynamic diameter of the droplets decreased with increasing the dye concentration, arising from enhanced electrostatic repulsion and alterations in the structure and arrangement of the surfactant molecules. While the PDI values indicated a relatively uniform size distribution within the system, more precise control over the synthesis conditions was required to minimize droplet aggregation and improve uniformity based on the observation of bimodal distributions in some measurements. The UV–Vis and fluorescence analyses revealed that the incorporation of Trypan Blue into the microemulsions can modify their optical properties.

The hypsochromic shift in the absorption region (λ_{max} = 562–594 nm), along with the increased emission intensity at higher MFD values indicated the residence of Trypan Blue in a less polar microenvironment. The small Stokes shifts further supported the dye's restricted media within the system.

Additionally, solvatochromic parameters were calculated, yielding $E_T(30)$ values of 48.1–50.9 kcal/mol and $\mu g/\mu e$ ratios close to unity, and demonstrating that the polarity of the aqueous core was influenced by droplet density.

Nevertheless, this trend was not observed consistently under all conditions, and the anomalies in the $E_T(30)$ values may be attributed to the partial aggregation of Trypan Blue. Thus, the characterization results and solvatochromic analyses indicate that these microemulsions possess considerable tunability in terms of structural and optical features, making them a promising platform for further investigation.

Conflicts of interest

The authors declare that they have no conflict of interest.

References

[1] Ravera, F., Dziza, K., Santini, E., Cristofolini, L., & Liggieri, L. (2021). Emulsification and emulsion stability: The role of the interfacial properties. *Advances in Colloid and Interface Science*, *288*, 102344.

[2] Xiao, T., Ma, X., Hu, H., Xiang, F., Zhang, X., Zheng, Y., Zheng, Y., Dong, H., Adhikari, B., Wang, Q., Shi, A. (2025) Advances in emulsion stability: A review on mechanisms, role of emulsifiers, and applications in food. *Food Chemistry: X*, 102792.

[3] Tadros, T. F. (2013). Emulsion formation, stability, and rheology. *Emulsion formation and stability*, 1-75.

[4] Goodarzi, F., & Zendehboudi, S. (2019). A comprehensive review on emulsions and emulsion stability in chemical and energy industries. *The Canadian Journal of Chemical Engineering*, *97*(1), 281-309.

[5] Angardi, V., Ettehadi, A., & Yucel, O. (2022). Critical review of emulsion stability and characterization techniques in oil processing. *Journal of Energy Resources Technology*, *144*(4), 040801.

[6] Tartaro, G., Mateos, H., Schirone, D., Angelico, R., & Palazzo, G. (2020). Microemulsion Microstructure(s): A Tutorial Review. *Nanomaterials*, *10*(9), 1657.

[7] Gradzielski, M., Duvail, M., de Molina, P. M., Simon, M., Talmon, Y., & Zemb, T. (2021). Using microemulsions: formulation based on knowledge of their mesostructure.

Chemical reviews, *121*(10), 5671-5740.

[8] Li, L., Qu, J., Liu, W., Peng, B., Cong, S., Yu, H., Yu. H., Zhang, B., Li, Y. (2024). Advancements in characterization techniques for microemulsions: From molecular insights to macroscopic phenomena. *Molecules*, *29*(12), 2901.

[9] Kim, G. W., Yun, S., Jang, J., Lee, J. B., & Kim, S. Y. (2023). Enhanced stability, formulations, and rheological properties of nanoemulsions produced with microfludization for eco-friendly process. *Journal of Colloid and Interface Science*, *646*, 311-319.

[10] Mitra, D. (2023). Microemulsion and its application: An inside story. *Materials Today: Proceedings*, *83*, 75-82.

[11] Journal of Pharmaceutical Research Science & Technology, (2020). Microemulsions-A Review. *Internationale Pharmaceutica Sciencia*. https://doi.org/10.31531/2231-5896.1000105

[12] Porras, M., Solans, C., Gonzalez, C., & Gutiérrez, J. M. (2008). Properties of water-in-oil (W/O) nano-emulsions prepared by a low-energy emulsification method. *Colloids and Surfaces A: Physicochemical and Engineering Aspects*, *324*(1-3), 181-188.

[13] Walters, S. H., Birchfield, A. S., & Fuglestad, B. (2024). Advances in utilizing reverse micelles to investigate membrane proteins. *Biochemical Society Transactions*, *52*(6), 2499-2511.

[14] Tiwary, L. K. (2013). Reverse Microemulsions as a Novel Reaction Media. *Oriental Journal of Chemistry*, *29*(1), 375.

[15] Mehta, D., Rathod, H., & Shah, D. P. (2015). Microemulsions: A potential novel drug delivery system. *Int. J. Pharm. Sci. 1(1)*, 48-60.

[16] Moulik, S. P., Rakshit, A. K., & Naskar, B. (2024). Physical chemical properties of surfactants in solution and their applications: A comprehensive account. *Journal of Surfactants and Detergents*, *27*(6), 895-925.

[17] Moulik, S. P., Chakraborty, I., & Rakshit, A. K. (2022). Role of surface-active materials (amphiphiles and surfactants) in the formation of nanocolloidal dispersions, and their applications. *Journal of Surfactants and Detergents*, *25*(6), 703-727.

[18] Sarkar, R., Pal, A., Rakshit, A., & Saha, B. (2021). Properties and applications of amphoteric surfactant: A concise review. *Journal of Surfactants and Detergents*, *24*(5), 709-730.

[19] Kronberg, B., Holmberg, K., & Lindman, B. (2014). Types of surfactants, their synthesis, and applications. *Surface chemistry of surfactants and polymers*, 1-47.

[20] Ghosh, S., Ray, A., & Pramanik, N. (2020). Self-assembly of surfactants: An overview on general aspects of amphiphiles. *Biophysical Chemistry*, *265*, 106429.

[21] Han, L., Luan, H., Ren, J., Zhang, Q., Xu, C., Li, G., Xiao, H., Zhou, Z., Zhang, L., Zhang, L. (2023). Effect of double chain anionic surfactant on the dynamic interfacial tensions of betaine solutions. *Journal of Molecular Liquids*, *382*, 121866.

[22] Crowder, M., Tahiry, F., Lizarraga, I., Rodriguez, S., Peña, N., & Sharma, A. K. (2023). Computational analysis of water dynamics in AOT reverse micelles. *Journal of Molecular Liquids*, *375*, 121340.

[23] Lunev, I. V., Turanov, A. N., Klimovitskaya, M. A., Galiullin, A. A., Zueva, O. S., & Zuev, Y. F. (2025). The Relaxation Behavior of Water Confined in AOT-Based Reverse Micelles Under Temperature-Induced Clustering. *International Journal of Molecular Sciences*, *26*(15), 7152.

[24] Hensel, J. K., Carpenter, A. P., Ciszewski, R. K., Schabes, B. K., Kittredge, C. T., Moore, F. G., & Richmond, G. L. (2017). Molecular characterization of water and surfactant AOT at nanoemulsion surfaces. *Proceedings of the National Academy of Sciences*, *114*(51), 13351-13356.

[25] Tan, Z., Zhang, Y., Dai, C., Li, L., Li, Y., & Xie, X. A. (2022). Investigation of AOT/isooctane/water reverse microemulsion system with the presence of different mass ratios of SDS: Conductivity and water solubilization. *Colloids and Surfaces A: Physicochemical and Engineering Aspects*, *648*, 129271.

[26] Rahdar, A., & Almasi-Kashi, M. (2017). Dynamic and spectroscopic studies of nano-micelles comprising dye in water/dioctyl sodium sulfosuccinate/decane droplet microemulsion at constant water content. *Journal of Molecular Structure*, *1128*, 257-262.

[27] Rahdar, A., Almasi-Kashi, M., & Aliahmad, M. (2017). Effect of chain length of oil on location of dye within AOT nanometer-sized droplet microemulsions at constant water content. *Journal of Molecular Liquids*, *233*, 398-402.

[28] Rahdar, A., & Almasi-Kashi, M. (2016). Photophysics of Rhodamine B in the nanosized water droplets: A concentration dependence study. *Journal of Molecular Liquids*, *220*, 395-403.

[29] Beri, D., Budiman, S., Sudiar, N. Y., Yusra, A., Erianjoni, E., Ganefri, G., & Amran, A. (2022). Fabrication of ballpoint-ink via encapsulating inorganic pigments in microemulsion gels. *RSC advances*, *12*(38), 24640-24646.

[30] Moradi, M., Saadat Jo, Z. (2026) Design and simulation of a highly sensitive plasmonic sensor based on graphene and black phosphorus strips, Pioneering Advances in Materials 2 (1), 1-10.

[31] Moradi, M., Ayareh, Z. (2022) Nanoplasmonic sensor chip fabricated based on au nanoparticles: effect of graphene oxide and reduced graphene oxide, Plasmonics 17 (4), 1437-1444

[32] Liu, Y., Hou, Z., Yang, J., & Gao, Y. (2015). Effects of antioxidants on the stability of β-Carotene in O/W emulsions stabilized by Gum Arabic. *J. Food Sci. Technol.*, *52*(6), 3300-3311. https://doi.org/10.1007/s13197-014-1380-0

[33] Wolski, R., Bazan-Wozniak, A., Nosal-Wiercinska, A., & Pietrzak, R. (2024). Methylene blue and rhodamine b dyes' efficient removal using biocarbons developed from waste. *Molecules*, *29*(17), 4022.

[34] Paul, R., Solans, C., & Erra, P. (2005). Study of a natural dye solubilisation in o/w microemulsions and its dyeing behaviour. *Colloids and Surfaces A: Physicochemical and Engineering Aspects*, *253*(1-3), 175-181.

[35] Malode, M. G. P., Chauhan, S. A., Bartare, S. A., Malode, L. M., Manwar, J. V., & Bakal, R. L. (2021). A critical review on nanoemulsion: Advantages, techniques and characterization. *Journal of Applied Pharmaceutical Sciences and Research*, *4*(3), 6-12.

[36] Roohinejad, S., Oey, I., Wen, J., Lee, S. J., Everett, D. W., & Burritt, D. J. (2015). Formulation of oil-in-water β-carotene microemulsions: Effect of oil type and fatty acid chain length. *Food chemistry*, *174*, 270-278.

[37] Mitra, D. (2023). Microemulsion and its application: An inside story. *Materials Today: Proceedings*, *83*, 75-82.

[38] Clark, S., Fletcher, P. D., & Ye, X. (1990). Interdroplet exchange rates of water-in-oil and oil-in-water microemulsion droplets stabilized by pentaoxyethylene monododecyl ether. *Langmuir*, *6*(7), 1301-1309.

[39] Jhanji, V., Chan, E., Das, S., Zhang, H., & Vajpayee, R. B. (2011). Trypan blue dye for anterior segment surgeries. *Eye*, *25*(9), 1113-1120.

[40] Avelar-Freitas, B. A., Almeida, V. G., Pinto, M. C. X., Mourao, F. A. G., Massensini, A. R., Martins-Filho, O. A., Rocha-Vieira, E., Brito-Melo, G. E. A. (2014). Trypan blue exclusion assay by flow cytometry. *Brazilian journal of medical and biological research*, *47*(4), 307-315.

[41] Strober, W. (2015). Trypan blue exclusion test of cell viability. *Current protocols in immunology*, *111*(1), A3-B.

[42] Jacob, S., Agarwal, A., Agarwal, A., Agarwal, S., Chowdhary, S., Chowdhary, R., & Bagmar, A. A. (2002). Trypan blue as an adjunct for safe phacoemulsification in eyes with white cataract. *Journal of Cataract & Refractive Surgery*, *28*(10), 1819-1825.